metals

MDPI

Article

Isothermal Sections of the Ni-Cr-Ta Ternary System at 1200 °C and 1300 °C

Cuiping Wang [1,*], Yuhui Liang [1], Shuiyuan Yang [1], Mujin Yang [1], Lingling Li [1], Jiajia Han [1], Yong Lu [1] and Xingjun Liu [1,2,3,*]

1 College of Materials and Fujian Provincial Key Laboratory of Materials Genome, Xiamen University, Xiamen 361005, China
2 State Key Laboratory of Advanced Welding and Joining, Harbin Institute of Technology, Harbin 150001, China
3 Institute of Materials Genome and Big Data, Harbin Institute of Technology, Shenzhen 518055, China
* Correspondence: wangcp@xmu.edu.cn (C.W.); lxj@xmu.edu.cn (X.L.); Tel.: +86-592-2187888 (X.L.); Fax: +86-592-2187966 (X.L.)

Received: 14 June 2019; Accepted: 5 July 2019; Published: 10 July 2019

Abstract: Two isothermal sections of the Ni-Cr-Ta ternary system at 1200 °C and 1300 °C have been determined by using electron probe microanalysis, energy dispersive spectroscopy and differential scanning calorimeter. A Laves phase (Ni, Cr)$_2$Ta(HT)(C14 structure) with large solid solubility stabilized by the Ni addition was determined in both two isothermal sections. The composition range of this phase was about 25.8–66.0 at.% Cr, 2.5-44.3 at.% Ni, and 24.0-40.0 at.% Ta at 1200 °C, which increased with raising temperature. The melting point of the Ni-Cr alloys decreased with the addition of Ta. No ternary compound was found in both these two isothermal sections. The present work could be significant for practical application of nickel-based alloys and future thermodynamics assessment of the Ni-Cr-Ta ternary system.

Keywords: Ni–Cr–Ta system; isothermal section; electron probe microanalysis

1. Introduction

Nickel-based superalloys have been applied in the aerospace field due to their excellent high-temperature properties, oxidation and corrosion resistance in the extreme harsh environment [1,2]. However, with higher industrial requirements in the structure materials for high-temperature applications in aviation field, materials capable of better mechanical strength, oxidation and corrosion resistance are required. In order to improve the properties of Ni-based alloys, an excellent alternative is to alloy refractory elements [3–6]. Technologically, Cr addition could significantly improve the oxidation and hot-corrosion resistance for the nickel-based alloys by forming a stable oxidation protective layer Cr_2O_3 at elevated temperatures [4,7–9]. Meanwhile, as a solid solution strengthening element, the alloying of Ta also improves the hot-corrosion and oxidation resistance [10,11]. However, the stabilization of topologically close packed (TCP) phase will deteriorate the mechanical properties of the superalloys for excessive addition of Cr and Ta elements [12,13]. Therefore, it is of significant necessity to investigate the phase diagram of the ternary Ni-Cr-Ta system, not only for the future thermodynamics assessment, but also enhancing the potential practical applications.

The Ni-Cr-Ta ternary system consisting of three binary subsystems, Ni-Cr, Ni-Ta, Cr-Ta, is illustrated in Figure 1. In 1986, Nash [14] reviewed the Ni-Cr system with a eutectic reaction at 1345 °C, where an extensive Ni terminal solid solution (face centered cubic) region and a less extensive Cr terminal solid solution (body centered cubic) region were identified. Additionally, Lee [15] and Zhu et al. [16] re-evaluated the Ni-Cr binary system, which is in agreement with the experimental results with the work of Nash.

The Ni-Ta binary system has been investigated by many researchers [17–30]. In 2018, Zhou et al. [30] reviewed the Ni-Ta system, where only four intermetallic compounds Ni_2Ta, Ni_3Ta, NiTa, $NiTa_2$, and two terminal solid solutions fcc-(Ni), bcc-(Ta) coexisted, and the Ni_8Ta was confirmed to be a metastable phase. There are two eutectic reactions, three peritectic reactions, a peritectoid reaction and a congruent transformation in this system. Two eutectic reactions L → Ni_3Ta + fcc-(Ni) and L → Ni_2Ta + Ni_6Ta_7 occurred at 1330 °C and 1350 °C, respectively. The Ni_6Ta_7 and $NiTa_2$ phase formed from two peritectic reactions. In addition, several investigators [23–28] have assessed the thermodynamic database of this binary system with CALPHAD method and first-principles calculation.

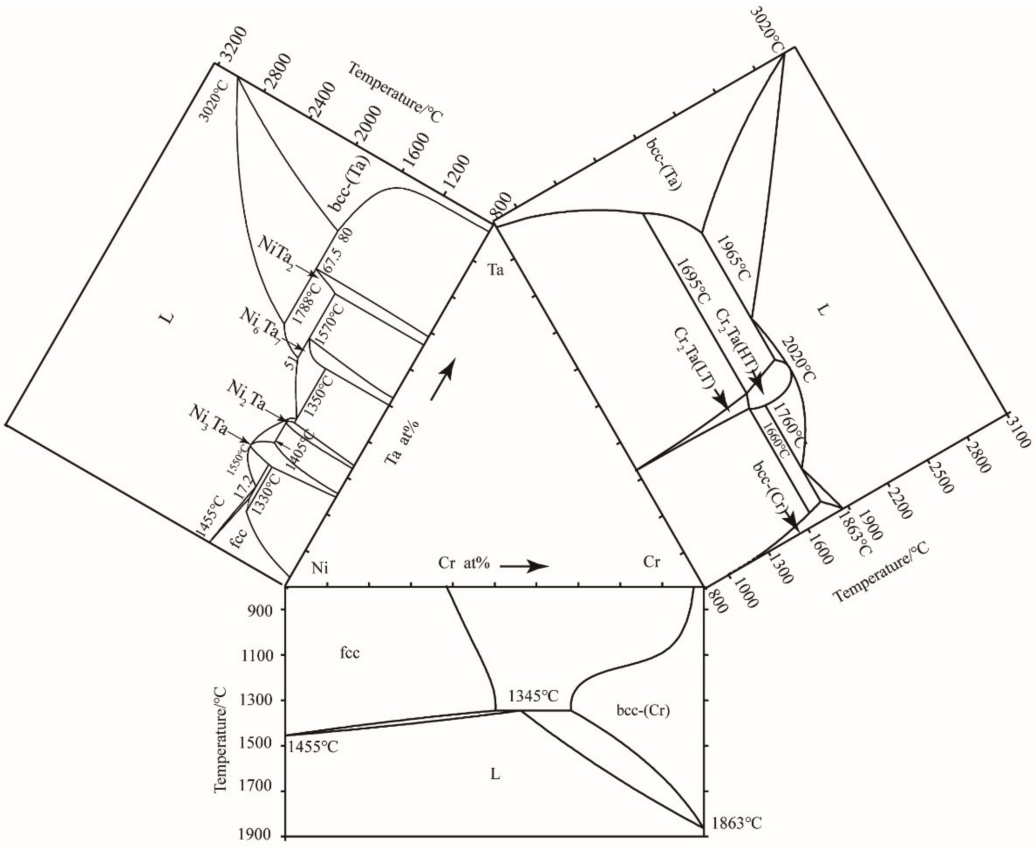

Figure 1. Binary phase diagrams constituting the Ni-Cr-Ta ternary system [14,30,31].

In 1987, Venkatraman et al. [32] reviewed the Cr-Ta system, in which two terminal solid solutions bcc-(Cr), bcc-(Ta) and intermediate phase Cr_2Ta formed from eutectic reaction occurred at 1760 and 1965 °C, respectively. The intermediate compound Cr_2Ta exhibits two Laves phase modifications. The high-temperature form, Cr_2Ta (HT), has the hexagonal $MgZn_2$-type (C14) structure, while the low-temperature form, Cr_2Ta (LT), has the cubic $MgCu_2$-type (C15) structure. In 1996, Okamoto [33] had redrawn this binary phase diagram based on the Venkatraman's work with an adjustment in the form of Cr_2Ta solidus complying with the Gibbs-Konovalov rule. In 1991, Kaufman et al. [23] assessed the Cr-Ta system with CALPHAD approach, then, Dupin et al. [34] re-evaluated the thermodynamic information based on the experimental results and the assessment of Kaufman. Recently, Pavlů et al. [31] re-modeled the Laves phases in the system using first-principles calculation and re-optimized the phase diagram with CALPHAD method.

As for the Ni-Cr-Ta ternary system, Nash et al. [35] investigated the phase equilibria in the Ni-rich portion of this system at 1000 °C and 1250 °C to establish a ternary Laves phase NiCrTa (the lattice parameter, a = 4.844 Å, c = 7.89 Å, annealed at 1250 °C, and a = 4.885 Å, c = 7.888 Å, annealed at 1000 °C) with hexagonal $MgZn_2$-type (C14) structure using electron microprobe and X-ray diffraction analysis. In 1985, Schittny et al. [36] reconfirmed the ternary compound NiCrTa in the partial isothermal section

at 1000 °C with concentration range of 0–40 at. % Ta. However, there is no ternary compound except for a Laves phase Cr_2Ta (hexagonal, $MgZn_2$-type, a = 4.844 Å, c = 7.9091 Å) in the isothermal section at 1100 °C, according to Nikolaev's et al. experimental phase diagram [37]. Additionally, Dupin et al. assessed the thermodynamic database of the Ni-Cr-Ta system [38]. The stable phases in the ternary Ni-Cr-Ta system are listed in the Table 1.

Table 1. The stable solid phases in the Ni-Cr-Ta ternary system.

System	Phase	Pearson Symbol	Prototye	Space Group	Strukturbericht	Ref.
Ni-Cr	fcc	*cF4*	Cu	*Fm-3m*	*A*1	[14]
	bcc-(Cr)	*cI*2	W	*Im-3m*	*A*2	[14]
	Ni_2Cr	*oP6*	Pt_2Mo			[14]
Ni-Ta	fcc	*cF4*	Cu	*Fm-3m*	*A*1	[30]
	bcc-(Ta)	*cI*2	W	*Im-3m*	*A*2	[30]
	Ni_3Ta	*tI8*	$TiAl_3$	*I4/mmm*	$D0_{22}$	[30]
		mP16	$NbPt_3$	$P2_1/m$		[30]
		oP8	Cu_3Ti	*Pmmn*	$D0_a$	[30]
	Ni_2Ta	*tI6*	$MoSi_2$	*I4/mmm*	$C11_b$	[30]
	Ni_6Ta_7	*hP*13	Fe_7W_6	*R-3m*	$D8_5$	[30]
	$NiTa_2$	*tI12*	Al_2Cu	*I4/mcm*	C16	[30]
Cr-Ta	bcc-(Cr)	*cI*2	W	*Im-3m*	*A*2	[31]
	bcc-(Ta)	*cI*2	W	*Im-3m*	*A*2	[31]
	Cr_2Ta(HT)	*hP12*	$MgZn_2$	*P63/mmc*	C14	[31]
	Cr_2Ta(LT)	*cF24*	$MgCu_2$	*Fd-3m*	C15	[31]

2. Experimental Details

High purity metals nickel (99.9 wt. %), chromium (99.9 wt. %) and Tantalum (99.9 wt. %) were used as our raw material to obtain alloys. All the metals were well cleaned to avoid the input of impurity surface oxidation before melting. All alloys were displayed in the form of atomic ratios (at. %). The ingots, around 20 g, were re-melted at least four times to get the uniformity with less than 0.5 wt. % weight loss. The alloys were melted in a high purity argon atmosphere arc furnace with a non-consumable tungsten electrode on a water-cooled copper platform. Then, all specimens were individually sealed in silica capsules with high purity argon, annealed at 1200 °C for 35 days and 1300 °C for 15 days, respectively. Additionally, in order to prevent oxidation, we put some pure yttrium fillings in the quartz capsules. Some alloys with liquid phase at 1300 °C were wrapped in the pure tantalum foil to avoid contact reaction with quartz.

All alloys were water quenched after heat treatment and well prepared for metallographic analysis. The equilibrium compositions of phases in the specimens were determined by electron probe microanalysis (EPMA) with 20 kV accelerating voltage and 1.0×10^{-8} A probe current. Additionally, the equilibrium compositions of liquid phases in some alloys annealed at 1300 °C were measured by energy dispersive spectroscopy (DSC) with 20 kV accelerating voltage and 2.0×10^{-9} A probe current. The crystal structure was identified by a Phillips Panlytical X-pert diffractometer using Cu-Kα radiation with 40 kV voltage and 40 mA current. The results were measured in the range of 2θ from 20° to 90° with a step interval of 0.015308° and a count time of 0.3 s per step. The melting points of some alloys were determined by differential scanning calorimeter (DSC) with a heating and cooling rate of 10 °C/min.

3. Results and Discussion

3.1. Microstructure

The phase relationship of the Ni-Cr-Ta ternary system at 1200 °C was established from 33 alloys annealed for 35 days. The nominal compositions of alloys and compositions of different phases at equilibrium are displayed in the Table 2. Meanwhile, the microstructure and XRD results of typical alloys annealed at 1200 °C for 35 days are presented in Figures 2 and 3, respectively.

Table 2. Equilibrium compositions of each phase in the Ni-Cr-Ta ternary alloys annealed at 1200 °C for 35 days.

Nominal Alloys (at. %)	Phase Equilibrium	Composition (at. %)					
	Phase 1/Phase 2/Phase 3	Phase 1		Phase 2		Phase 3	
		Cr	Ta	Cr	Ta	Cr	Ta
$Ni_{54}Cr_{43.5}Ta_{2.5}$	fcc	43.4	53.9				
$Ni_{80.5}Cr_7Ta_{12.5}$	fcc/Ni_3Ta	8.5	10	3.3	19.9		
$Ni_{59}Cr_{33}Ta_8$	fcc/Ni_3Ta	41.5	5.0	3.0	21.7		
$Ni_{14}Cr_{65}Ta_{21}$	bcc-(Cr)/(Ni, Cr)$_2$Ta(HT)	97.0	0.4	50.8	30.0		
$Ni_{46}Cr_{33}Ta_{21}$	bcc-(Cr)/(Ni, Cr)$_2$Ta(HT)/Ni_3Ta	81.5	0.9	33	23.4	3.4	22.4
$Ni_{65}Cr_5Ta_{30}$	Ni_3Ta/Ni_2Ta/(Ni, Cr)$_2$Ta(HT)	0.6	25.1	1.6	37.3	26.5	31.9
$Ni_{40}Cr_{22}Ta_{38}$	Ni_6Ta_7/(Ni, Cr)$_2$Ta(HT)	10.8	45	27.8	34.8		
$Ni_{30}Cr_{31}Ta_{39}$	Ni_6Ta_7/(Ni, Cr)$_2$Ta(HT)	20.7	45.2	36.3	35.8		
$Ni_{21}Cr_{33}Ta_{46}$	Ni_6Ta_7/(Ni, Cr)$_2$Ta(HT)	28.4	48	44.8	38.3		
$Ni_{39}Cr_4Ta_{57}$	Ni_6Ta_7/$NiTa_2$	6.5	52.7	0.2	64.5		
$Ni_{13}Cr_7Ta_{80}$	$NiTa_2$/bcc-(Ta)	12	62.2	4.0	95.2		
$Ni_{33}Cr_{34}Ta_{33}$	(Ni, Cr)$_2$Ta(HT)	34.5	33.0				
$Ni_{78}Cr_9Ta_{13}$	fcc/Ni_3Ta	11.4	8.3	1.9	21.9		
$Ni_{53}Cr_{37}Ta_{10}$	fcc/Ni_3Ta/bcc-(Cr)	41.9	4.6	3.6	22.5	80.3	0.6
$Ni_{38}Cr_{32}Ta_{30}$	(Ni, Cr)$_2$Ta(HT)	31.9	29.5				
$Ni_{25}Cr_{37}Ta_{38}$	Ni_6Ta_7/(Ni, Cr)$_2$Ta(HT)	15.5	48.5	38.6	35.6		
$Ni_{64}Cr_7Ta_{29}$	Ni_3Ta/Ni_2Ta/(Ni, Cr)$_2$Ta(HT)	0.5	24.9	1.8	37.1	26.6	32.1
$Ni_{53}Cr_8Ta_{39}$	Ni_6Ta_7/Ni_2Ta/(Ni, Cr)$_2$Ta(HT)	9.6	46.1	0.8	33.5	26.8	33.2
$Ni_2Cr_{75}Ta_{23}$	bcc-(Cr)/(Ni, Cr)$_2$Ta(HT)	98.6	0.7	66.7	30.8		
$Ni_9Cr_{48}Ta_{43}$	Ni_6Ta_7/(Ni, Cr)$_2$Ta(HT)	40.1	50	54.1	39.6		
$Ni_{27}Cr_{41}Ta_{32}$	(Ni, Cr)$_2$Ta(HT)	40.9	32.1				
$Ni_{26}Cr_{57}Ta_{17}$	Ni_6Ta_7/bcc-(Ta)	19.1	53.8	6.2	93.7		
$Ni_{35}Cr_{53}Ta_{12}$	bcc-(Cr)/(Ni, Cr)$_2$Ta(HT)/Ni_3Ta	81.3	0.9	33.5	23.7	3.2	22.5
$Ni_{27}Cr_{53}Ta_{20}$	bcc-(Cr)/(Ni, Cr)$_2$Ta(HT)	92.8	0.2	36.9	25.9		
$Ni_{23}Cr_{53}Ta_{24}$	bcc-(Cr)/(Ni, Cr)$_2$Ta(HT)	96.3	0.5	45.3	28.9		
$Ni_{22}Cr_{45}Ta_{33}$	(Ni, Cr)$_2$Ta(HT)	45.2	32.9				
$Ni_{13}Cr_{53}Ta_{34}$	(Ni, Cr)$_2$Ta(HT)	53.1	34				
$Ni_{16}Cr_{38}Ta_{46}$	Ni_6Ta_7/(Ni, Cr)$_2$Ta(HT)	33.3	49.8	51	38.9		
$Ni_{12}Cr_{33}Ta_{55}$	Ni_6Ta_7/bcc-(Ta)	35.6	52.1	6.8	93.1		
$Ni_{15}Cr_{19}Ta_{66}$	Ni_6Ta_7/bcc-(Ta)	24.4	55.1	6.4	93.5		
$Ni_{36}Cr_{58}Ta_6$	fcc/Ni_3Ta/bcc-(Cr)	41.8	4.5	3.4	22.3	80.1	0.5
$Ni_5Cr_{40}Ta_{55}$	Ni_6Ta_7/(Ni, Cr)$_2$Ta(HT)/bcc-(Ta)	39.2	51.5	58.7	38.5	6.3	93.5
$Ni_{10}Cr_{25}Ta_{65}$	Ni_6Ta_7/bcc-(Ta)	30.5	52.4	5.4	93.2		

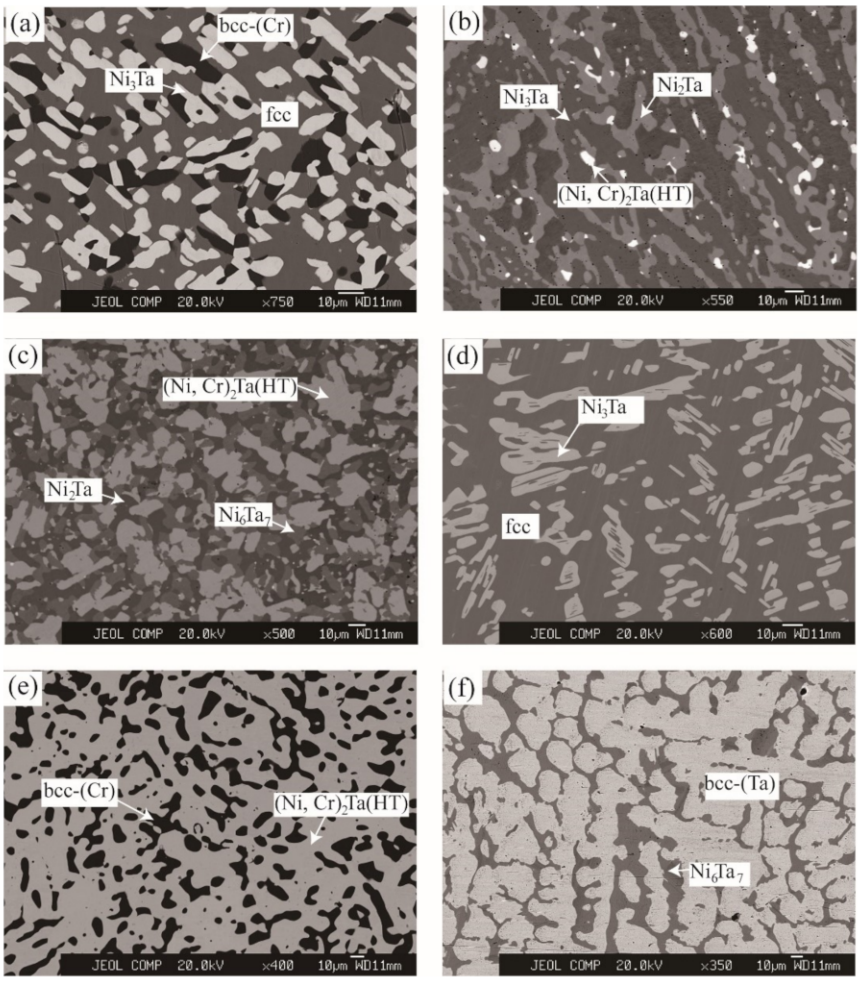

Figure 2. The microstructure of typical alloys in the Ni-Cr-Ta system annealed at 1200 °C for 35 days. (**a**) $Ni_{53}Cr_{37}Ta_{10}$; (**b**) $Ni_{64}Cr_7Ta_{29}$; (**c**) $Ni_{53}Cr_8Ta_{39}$; (**d**) $Ni_{59}Cr_{33}Ta_8$; (**e**) $Ni_{27}Cr_{53}Ta_{20}$; (**f**) $Ni_{12}Cr_{33}Ta_{55}$.

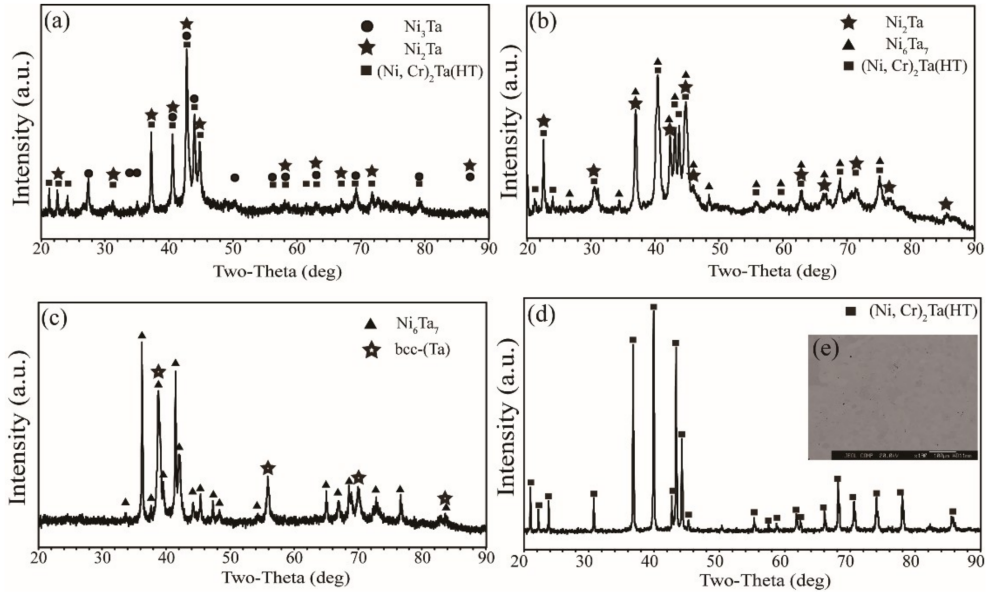

Figure 3. The XRD patterns of typical alloys in the Ni-Cr-Ta system annealed at 1200 °C for 35 days. (**a**) $Ni_{64}Cr_7Ta_{29}$; (**b**) $Ni_{53}Cr_8Ta_{39}$; (**c**) $Ni_{12}Cr_{33}Ta_{55}$; (**d**) $Ni_{13}Cr_{53}Ta_{34}$.

As presented in Figure 2a–c, the microstructure of three-phase regions was detected in these alloys. Figure 2a showed the three-phase equilibrium, two terminal solid solutions fcc, bcc-(Cr) and a compound Ni_3Ta, bright regions in the microstructure of the $Ni_{53}Cr_{37}Ta_{10}$ alloy. Figure 2b showed the three-phase equilibrium of the $Ni_{64}Cr_7Ta_{29}$ alloy, in which the white precipitated (Ni, Cr)$_2$Ta(HT) phase was uniformly distributed in the Ni_3Ta and Ni_2Ta phase. Moreover, the three-phase equilibrium state was identified by the XRD result in Figure 3a. Three-phase region, Ni_2Ta, Ni_6Ta_7 and (Ni, Cr)$_2$Ta(HT) was found in the $Ni_{53}Cr_8Ta_{39}$ alloy after annealed at 1200 °C for 35 days. Additionally, the XRD analysis in Figure 3b just confirmed the microstructure. As can be seen from Figure 2d–f, three two-phase regions were identified in these three alloys. Figure 2d showed the equilibrium of the gray matrix fcc and white Ni_3Ta phase in the $Ni_{59}Cr_{33}Ta_8$ alloy annealed at 1200 °C for 35 days. The phase relation of the $Ni_{27}Cr_{53}Ta_{20}$ alloy, a terminal solid solution bcc-(Cr) and a compound (Ni, Cr)$_2$Ta(HT), was described in Figure 2e. Furthermore, there was a two-phase section of white bcc-(Ta) and gray Ni_6Ta_7 phase in the $Ni_{12}Cr_{33}Ta_{55}$ alloy as illustrated in Figure 2f. Additionally, the crystal structure of the $Ni_{12}Cr_{33}Ta_{55}$ alloy was identified by the XRD result displayed in Figure 3c. Figure 3d showed the XRD result of a single (Ni, Cr)$_2$Ta(HT) phase in the $Ni_{13}Cr_{53}Ta_{34}$ alloy and the microstructure was displayed in the Figure 3e.

In the experiment, several alloys were designed to investigate phase relation of the Ni-Cr-Ta system at 1300 °C. Table 3 listed the alloys compositions and phase equilibrium compositions of the alloys annealed at 1300 °C. In addition, the microstructure and XRD patterns of typical alloys were presented in the Figures 4 and 5, respectively. Figure 4a,c showed two three-phase equilibriums with liquid phase. As presented in Figure 4a, the microstructure of three-phase region, gray liquid phase, black fcc phase and white Ni_3Ta phase, was determined in the $Ni_{59}Cr_{33}Ta_8$ alloy annealed at 1300 °C for 3 h. Figure 4c displayed the three-phase microstructure of liquid phase, oval-shaped bcc-(Cr) and (Ni, Cr)$_2$Ta(HT) phase in the $Ni_{35}Cr_{53}Ta_{12}$ alloy annealed at 1300 °C for 3 h. There was a three-phase section, black matrix Ni_3Ta, white precipitated Ni_2Ta and gray (Ni, Cr)$_2$Ta(HT) identified in the $Ni_{65}Cr_5Ta_{30}$ alloy as shown in Figure 4b. Figure 4d,e illustrated two two-phase equilibrium. The Ni_6Ta_7 and (Ni, Cr)$_2$Ta(HT) phase were determined in the $Ni_{16}Cr_{38}Ta_{46}$ alloy described in Figure 4d, and the two-phase equilibrium was supported by the XRD result in Figure 5a. The microstructure of the $Ni_{12}Cr_{33}Ta_{55}$ alloy in Figure 4e was confirmed as bcc-(Ta) and Ni_6Ta_7 by the XRD pattern presented in Figure 5b. Figure 4f showed the three-phase region, bcc-(Ta), Ni_6Ta_7 and (Ni, Cr)$_2$Ta(HT), of the $Ni_5Cr_{40}Ta_{55}$ alloy, and the result was confirmed by the XRD pattern in Figure 5c. As shown in Figure 4d–e, the cracks and holes were observed in the brittle Laves phase Ni_6Ta_7.

Table 3. Equilibrium compositions of each phase in the Ni-Cr-Ta ternary alloys annealed at 1300 °C for 15 days or 3 h.

Nominal Alloys (at%)	Phase Equilibrium	Composition (at. %)					
	Phase 1/Phase 2/Phase 3	Phase 1		Phase 2		Phase 3	
		Cr	Ta	Cr	Ta	Cr	Ta
$Ni_{54}Cr_{43.5}Ta_{2.5}$	fcc	46.0	2.4				
$Ni_{59}Cr_{33}Ta_{8}$ *	fcc/Ni_3Ta/L	34.3	6.6	3.7	22.4	37.5	11.7
$Ni_{14}Cr_{65}Ta_{21}$	bcc-(Cr)/(Ni, Cr)$_2$Ta(HT)	95.5	0.6	51.6	29.6		
$Ni_{46}Cr_{33}Ta_{21}$ *	L/(Ni, Cr)$_2$Ta(HT)/Ni_3Ta	35.1	15.9	33.0	24.6	3.3	23.8
$Ni_{65}Cr_{5}Ta_{30}$	Ni_3Ta/Ni_2Ta/(Ni, Cr)$_2$Ta(HT)	0.6	23.6	1.0	31.3	22.4	31.9
$Ni_{40}Cr_{22}Ta_{38}$	Ni_6Ta_7/(Ni, Cr)$_2$Ta(HT)	11.6	45.5	22.9	35.2		
$Ni_{30}Cr_{31}Ta_{39}$	Ni_6Ta_7/(Ni, Cr)$_2$Ta(HT)	18.9	46.7	36.5	35.6		
$Ni_{21}Cr_{33}Ta_{46}$	Ni_6Ta_7/(Ni, Cr)$_2$Ta(HT)	27.7	48.3	45.1	38.2		
$Ni_{39}Cr_{4}Ta_{57}$	Ni_6Ta_7/$NiTa_2$	0.5	65.5	7.2	55		
$Ni_{13}Cr_{7}Ta_{80}$	$NiTa_2$/bcc-(Ta)	12.0	58.2	4.7	94.5		
$Ni_{33}Cr_{34}Ta_{33}$	(Ni, Cr)$_2$Ta(HT)	34.5	33.1				
$Ni_{78}Cr_{9}Ta_{13}$	fcc	9.2	12.3				
$Ni_{53}Cr_{37}Ta_{10}$ *	fcc/L	38.4	6.5	36.9	13.5		
$Ni_{38}Cr_{32}Ta_{30}$	(Ni, Cr)$_2$Ta(HT)	32.2	30.2				
$Ni_{25}Cr_{37}Ta_{38}$	Ni_6Ta_7/(Ni, Cr)$_2$Ta(HT)	19.6	47.6	39.3	36.6		
$Ni_{64}Cr_{7}Ta_{29}$	Ni_3Ta/Ni_2Ta/(Ni, Cr)$_2$Ta(HT)	0.7	23.4	1.2	31.1	22.3	31.6
$Ni_{53}Cr_{8}Ta_{39}$	Ni_6Ta_7/Ni_2Ta/(Ni, Cr)$_2$Ta(HT)	8.5	45.4	0.2	32.7	17.4	36.5
$Ni_{2}Cr_{75}Ta_{23}$	bcc-(Cr)/(Ni, Cr)$_2$Ta(HT)	98.1	0.8	65.2	32.3		
$Ni_{9}Cr_{48}Ta_{43}$	Ni_6Ta_7/(Ni, Cr)$_2$Ta(HT)	42.3	50.2	54.3	40.6		
$Ni_{27}Cr_{41}Ta_{32}$	(Ni, Cr)$_2$Ta(HT)	41.0	31.8				
$Ni_{26}Cr_{57}Ta_{17}$	Ni_6Ta_7/bcc-(Ta)	19.8	54.0	5.1	94.3		
$Ni_{35}Cr_{53}Ta_{12}$ *	bcc-(Cr)/(Ni, Cr)$_2$Ta(HT)/L	82.8	0.9	37.5	24.4	39.8	12.4
$Ni_{27}Cr_{53}Ta_{20}$	bcc-(Cr)/(Ni, Cr)$_2$Ta(HT)	89.2	0.5	43.6	27.0		
$Ni_{23}Cr_{53}Ta_{24}$	bcc-(Cr)/(Ni, Cr)$_2$Ta(HT)	93.5	0.5	45.5	26.8		
$Ni_{22}Cr_{45}Ta_{33}$	(Ni, Cr)$_2$Ta(HT)	45.3	32.5				
$Ni_{13}Cr_{53}Ta_{34}$	(Ni, Cr)$_2$Ta(HT)	53.5	33.7				
$Ni_{16}Cr_{38}Ta_{46}$	Ni_6Ta_7/(Ni, Cr)$_2$Ta(HT)	35.7	48.8	49.8	39.4		
$Ni_{51}Cr_{28}Ta_{21}$ *	Ni_3Ta/(Ni, Cr)$_2$Ta(HT)/L	3.1	23.4	33.0	24.5	34.8	16.2
$Ni_{12}Cr_{33}Ta_{55}$	Ni_6Ta_7/bcc-(Ta)	36.9	51.0	5.4	94.1		
$Ni_{15}Cr_{19}Ta_{66}$	Ni_6Ta_7/bcc-(Ta)	26.8	53.3	5.3	93.8		
$Ni_{36}Cr_{58}Ta_{6}$ *	fcc/bcc-(Cr)/L	40.1	6.1	80.7	0.5	39.7	11.8
$Ni_{78}Cr_{12}Ta_{10}$	fcc/Ni_3Ta	13.4	9.7	3.2	21.5		
$Ni_{5}Cr_{40}Ta_{55}$	Ni_6Ta_7/(Ni, Cr)$_2$Ta(HT)/(Ta)	41.6	51.1	53.5	42.1	6.3	93.5
$Ni_{10}Cr_{25}Ta_{65}$	Ni_6Ta_7/bcc-(Ta)	29.8	54.6	6.8	93.1		

* Indicated that the alloy was annealed at 1300 °C for 3 h.

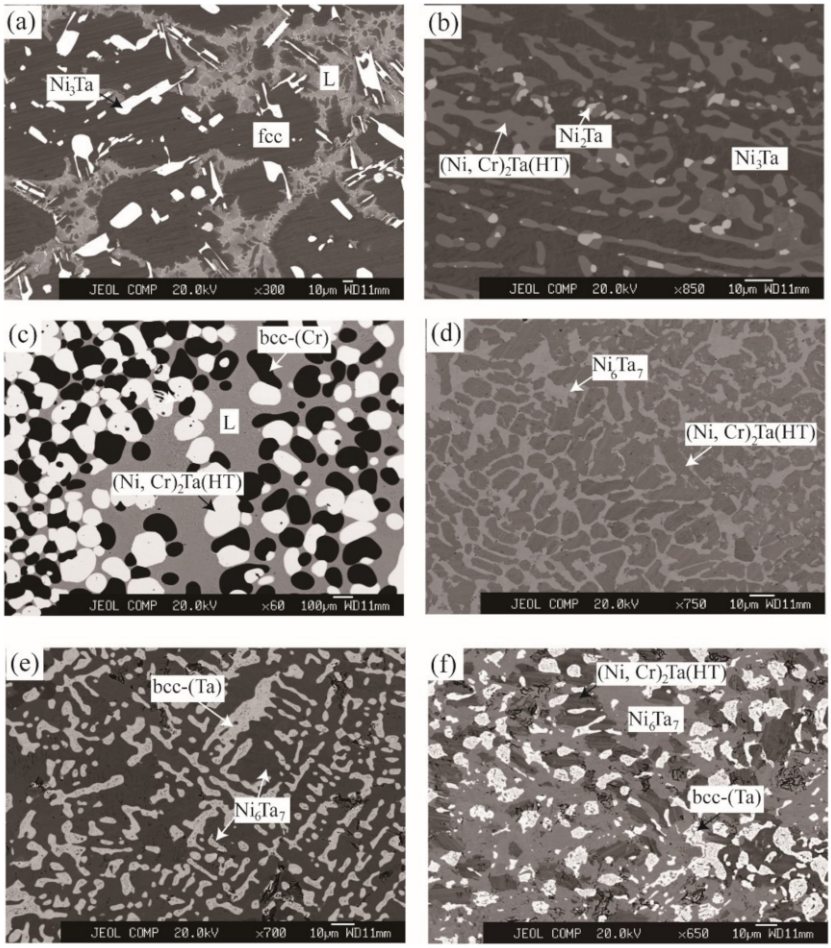

Figure 4. The microstructure of typical alloys in the Ni-Cr-Ta system annealed at 1300 °C. (**a**) $Ni_{59}Cr_{33}Ta_8$; (**c**) $Ni_{35}Cr_{53}Ta_{12}$ alloys annealed at 1300 °C for 3 h. (**b**) $Ni_{65}Cr_5Ta_{30}$; (**d**) $Ni_{16}Cr_{38}Ta_{46}$; (**e**) $Ni_{12}Cr_{33}Ta_{55}$; (**f**) $Ni_5Cr_{40}Ta_{55}$ alloys annealed at 1300 °C for 15 days.

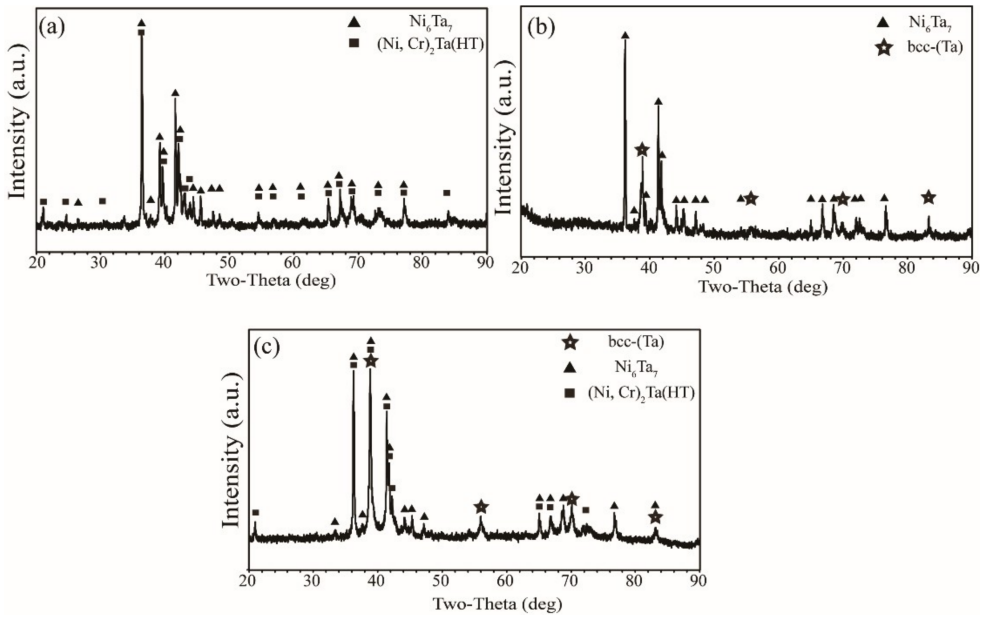

Figure 5. The XRD patterns of typical alloys in the Ni-Cr-Ta system annealed at 1300 °C for 15 days. (**a**) $Ni_{16}Cr_{38}Ta_{46}$; (**b**) $Ni_{12}Cr_{33}Ta_{55}$; (**c**) $Ni_5Cr_{40}Ta_{55}$.

3.2. Isothermal Sections

The measured equilibrium compositions of the Ni-Cr-Ta system at 1200 °C and 1300 °C were listed in the Tables 2 and 3, respectively. According to the experimental results, the isothermal sections of the Ni-Cr-Ta ternary system at 1200 °C and 1300 °C were established in Figures 6 and 7. At 1200 °C, there are eight stable solid phases, fcc, Ni_3Ta, Ni_2Ta, Ni_6Ta_7, $NiTa_2$, bcc-(Ta), bcc-(Cr), and $(Cr)_2Ta$(HT). Meanwhile, five three-phase regions, fcc + Ni_3Ta + bcc-(Cr), Ni_3Ta + bcc-(Cr) + (Ni, Cr)$_2$Ta(HT), Ni_3Ta + Ni_2Ta + (Ni, Cr)$_2$Ta(HT), Ni_2Ta + Ni_6Ta_7 + (Ni, Cr)$_2$Ta(HT) and Ni_6Ta_7 + bcc-(Ta) + (Ni, Cr)$_2$Ta(HT), were experimentally determined and marked as triangle with solid lines in present work. However, the other three three-phase equilibria, Ni_6Ta_7 + $NiTa_2$ + bcc-(Ta), bcc-(Cr) + $(Cr)_2Ta$(LT) + (Ni, Cr)$_2$Ta(HT) and bcc-(Ta) + $(Cr)_2Ta$(LT) + (Ni, Cr)$_2$Ta(HT), at 1200 °C were inferred and presented as triangle with dash lines. A single-phase region (Ni, Cr)$_2$Ta(HT) with hexagonal $MgZn_2$-type (C14) structure was detected with a large composition range of about 25.8-66.0 at. % Cr, 2.5-44.3 at. % Ni, and 24.0-40.0 at. % Ta, at 1200 °C. It should be noted that the (Ni, Cr)$_2$Ta(HT) appears in two isothermal sections of the Ni-Cr-Ta system in spite of the non-existence in Cr-Ta subsystem at two temperatures. Distinctly, the Ni addition to the Cr-Ta binary system stablizes the (Ni, Cr)$_2$Ta(HT) phase at low temperature. The Ni_3Ta and Ni_2Ta just dissolves a little of Cr, while the solubility of Cr in the Ni_6Ta_7 and $NiTa_2$ phase reaches up to 40.1 and 13.1 at. %, respectively. Despite the same crystal structure of Ta and Cr, the solubility of Ta/Cr in two bcc terminal solid solution is quite small.

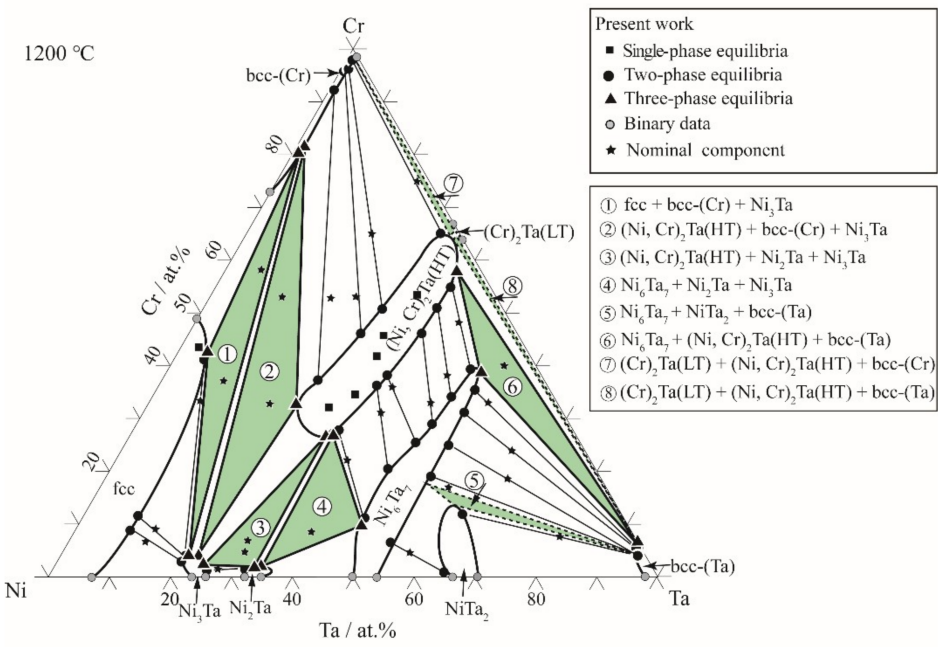

Figure 6. Experimentally determined isothermal section of the Ni-Cr-Ta system at 1200 °C.

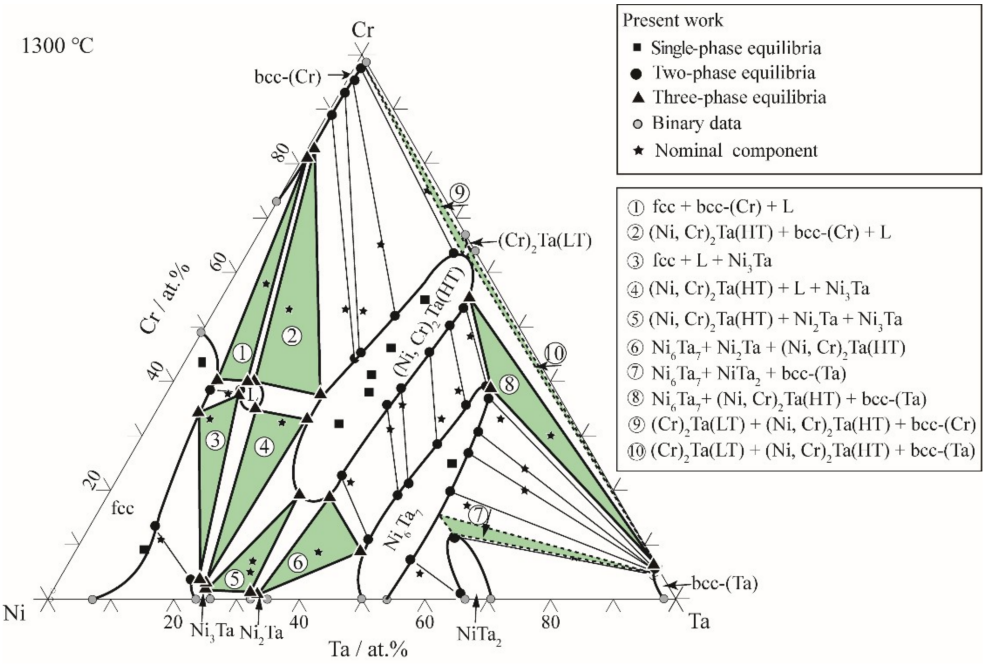

Figure 7. Experimentally determined isothermal section of the Ni-Cr-Ta system at 1300 °C.

The isothermal section at 1300 °C is shown in Figure 7, where with existence of liquid phase, two three-phase regions fcc + Ni_3Ta + bcc-(Cr) and Ni_3Ta + bcc-(Cr) + (Ni, Cr)$_2$Ta(HT) disappear and are replaced by four confirmed three-phase equilibria, fcc + bcc-(Cr) + L, fcc + Ni_3Ta + L, bcc-(Cr) + (Ni, Cr)$_2$Ta(HT) + L and Ni_3Ta + (Ni, Cr)$_2$Ta(HT) + L. The other three-phase regions are similar to the isothermal sections at 1200°C, where the three-phase equilibria, Ni_3Ta + Ni_2Ta + (Ni, Cr)$_2$Ta(HT), Ni_2Ta + Ni_6Ta_7 + (Ni, Cr)$_2$Ta(HT) and Ni_6Ta_7 + bcc-(Ta) + (Ni, Cr)$_2$Ta(HT), were determined and the other three were inferred. With the temperature rising to 1300 °C, a liquid phase was identified near the Ni-Cr side alloys. It is evident that the Ta addition to the Ni-Cr alloys decreases the melting point of the Ni-Cr eutectic alloys in consideration of the eutectic reaction L → Ni_{44} + Cr_{56} at 1345 °C.

3.3. The Liquid Region

As can be observed from the microstructure in Figure 4c and isothermal section at 1300 °C, a liquid phase was confirmed at 1300 °C. However, according to the experimental results in the three subsystems, no liquid phase exists at 1300 °C. In order to confirm the experimental results in the present work, the DSC analysis was conducted to obtain the melting point of the related alloys. On the basis of DSC result and microstructure in Figure 8, the bcc-(Cr) phase transformed to liquid phase as the temperature increased from 1200 °C to 1285 °C and the melting point of the bcc-(Cr) phase in the $Ni_{51}Cr_{28}Ta_{21}$ alloy was measured to be about 1237 °C. Owing to the liquid phase that appeared near the Ni-Cr side, we supposed that the Ta addition in Ni-Cr alloys decreases the temperature of the eutectic reaction, L → fcc + bcc-(Cr). The corresponding results indicate that the Ta addition reduces the melting point of the Ni-Cr alloys.

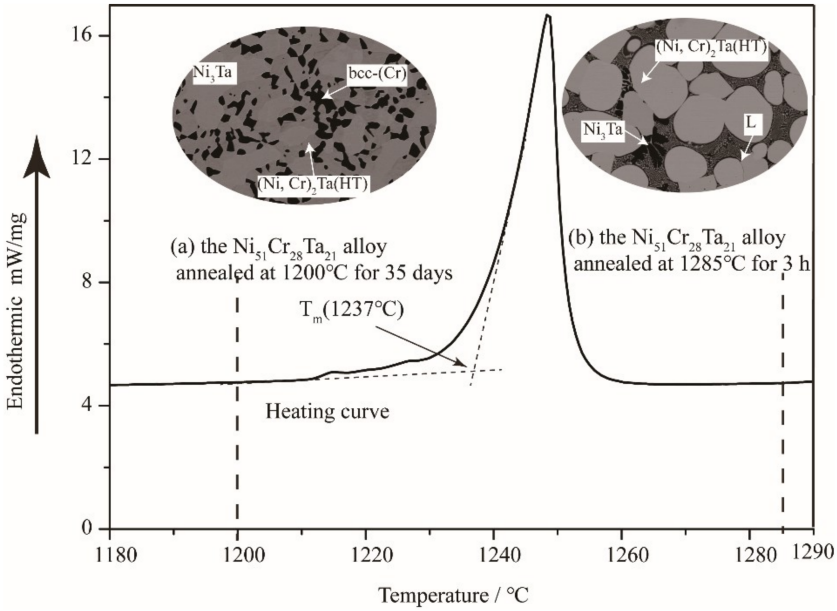

Figure 8. The heating curve of the $Ni_{51}Cr_{28}Ta_{21}$ alloy and microstructure annealed at (**a**) 1200 °C for 35 days; (**b**) 1285 °C for 3 h.

4. Conclusions

In the present work, the isothermal sections of the Ni-Cr-Ta ternary system at 1200 °C and 1300 °C were experimentally established. The corresponding results are shown as follows:

(1) The solubility of Cr in Ni_6Ta_7 phase was about 41.6 at. % at 1300 °C, and no ternary compound was found at two sections.

(2) The high temperature (Ni, Cr)$_2$Ta(HT) ($MgZn_2$-type) phase with a large composition range was determined at both two temperatures, which was stabilized by the Ni addition to Cr–Ta alloys against low temperature, and its solubility increased as temperature raise from 1200 °C to 1300 °C.

(3) A small liquid region was confirmed at 1300 °C, while it disappeared at 1200 °C. The results indicate that the addition of Ta reduced the melting point of the Ni–Cr alloys.

Author Contributions: Conceptualization, C.W. and X.L.; Investigation, Y.L. (Yuhui Liang), M.Y. and L.L.; Writing–Original Draft Preparation, Y.L. (Yuhui Liang); Writing-Review and Editing, S.Y., M.Y., J.H. and Y.L. (Yong Lu) Supervision, X.L. and C.W.; and Funding Acquisition, X.L. and C.W.

Funding: This research was founded by the National Natural Science Foundation of China (Grant No. 51831007) and the National Key R&D Program of China (Grant No. 2017YFB0702901).

Conflicts of Interest: The authors declare no conflict of interest.

References

1. Erickson, G.L. A new, third-generation, single-crystal, casting superalloy. *JOM* **1995**, *47*, 36–39. [CrossRef]
2. Pollock, T.M.; Tin, S. Nickel-based superalloys for advanced turbine engines: Chemistry, Microstructure and Properties. *J. Propul. Power* **2006**, *22*, 361–374. [CrossRef]
3. Jena, A.K.; Chaturvedi, M.C. The role of alloying elements in the design of nickel-base superalloys. *J. Matrl. Sci.* **1984**, *19*, 3121–3139. [CrossRef]
4. Xu, X.J.; Wu, Q.; Gong, S.K.; Li, S.S. Effect of Cr and Re on the oxidation resistance of Ni_3Al-base single crystal alloy IC21 at 1100 °C. *High Perform. Struct. Mater.* **2013**, *748*, 582–587.
5. Zheng, L.; Zhang, G.; Lee, T.L.; Gorley, M.J.; Wang, Y.; Xiao, C.; Li, Z. The effects of Ta on the stress rupture properties and microstructural stability of a novel Ni-base superalloy for land-based high temperature applications. *Mater. Des.* **2014**, *61*, 61–69. [CrossRef]

6. Huang, Y.; Mao, Z.; Noebe, R.D.; Seidman, D.N. The effects of refractory elements on Ni-excesses and Ni-depletions at γ(fcc)/γ'($L1_2$) interfaces in model Ni-based superalloys: Atom-probe tomographic experiments and first-principles calculations. *Acta Mater.* **2016**, *121*, 288–298. [CrossRef]
7. Eliaz, N.; Shemesh, G.; Latanision, R.M. Hot corrosion in gas turbine components. *Eng. Failure Anal.* **2002**, *9*, 31–43. [CrossRef]
8. Okazaki, M. High-temperature strength of Ni-base superalloy coatings. *Sci. Technol. Adv. Mater.* **2001**, *2*, 357–366. [CrossRef]
9. Hayes, J.R.; Gray, J.J.; Szmodis, A.W.; Orme, C.A. Influence of chromium and molybdenum on the corrosion of nickel-based alloys. *Corros. Sci.* **2006**, *62*, 491–500. [CrossRef]
10. Yang, S.W. Effect of Ti and Ta on the oxidation of a complex superalloy. *Oxid. Met.* **1981**, *15*, 375–397. [CrossRef]
11. Park, S.-J.; Seo, S.-M.; Yoo, Y.-S.; Jeong, H.-W.; Jang, H. Effects of Al and Ta on the high temperature oxidation of ni-based superalloys. *Corros. Sci.* **2015**, *90*, 305–312. [CrossRef]
12. Acharya, M.V.; Fuchs, G.E. The effect of long-term thermal exposures on the microstructure and properties of CMSX-10 single crystal Ni-base superalloys. *Mater. Sci. Eng. A* **2004**, *381*, 143–153. [CrossRef]
13. Pigrova, G.D. TCP-phases in nickel-base alloys with elevated chromium content. *Met. Sci. Heat Treat.* **2005**, *47*, 544–551. [CrossRef]
14. Nash, P. The Cr-Ni (chromium-nickel) system. *Bull. Alloy Phase Diagrams* **1986**, *7*, 466–476. [CrossRef]
15. Lee, B.-J. On the stability of Cr carbides. *Calphad* **1992**, *16*, 121–149. [CrossRef]
16. Zhu, N.; Li, J.; Lu, X.-G.; He, Y.; Zhang, J. Experimental and Computational study of diffusion mobilities for fcc Ni-Cr-Mo alloys. *Metall. Mater. Trans. A* **2015**, *46*, 5444–5455. [CrossRef]
17. Kripyakevich, P.I.; Pylaeva, E.N. Crystal structure of the compound Ta_2Ni. *J. Struct. Chem.* **1962**, *3*, 35–37. [CrossRef]
18. Giessen, B.C.; Grant, N.J. The crystal structure of $TaNi_3$ and its change on cold working. *Acta Metall.* **1967**, *15*, 871–877. [CrossRef]
19. Larson, J.M.; Taggart, R.; Polonis, D.H. Ni_8Ta in Nickel-rich Ni-Ta alloys. *Metall. Mater. Trans. B* **1970**, *1*, 485–489. [CrossRef]
20. Saburi, T.; Nakamura, M.; Nenno, S. Crystal structure and twin lamellae of Ni_3Ta. *J. Less-Common Met.* **1975**, *41*, 135–139. [CrossRef]
21. Nash, P.; West, D.R.F. Ni-Al and Ni-Ta phase diagrams. *Met. Sci.* **1983**, *17*, 99–100. [CrossRef]
22. Nash, A.; Nash, P. The Ni-Ta system. *J. Phase Equilib.* **1984**, *5*, 444–445. [CrossRef]
23. Kaufman, L. Coupled thermochemical and phase diagram data for tantalum based binary alloys. *Calphad* **1991**, *15*, 243–259. [CrossRef]
24. Ansara, I.; Selleby, M. Thermodynamic analysis of the Ni-Ta system. *Calphad* **1994**, *18*, 99–107. [CrossRef]
25. Cui, Y.; Jin, Z. Experimental study and reassessment of the Ni-Ta binary system. *Z. Metallkd.* **1999**, *90*, 233–241.
26. Pan, X.; Jin, Z. Experimental determination and Re-optimization of Ni-Ta binary system. *Trans. Nonferrous Met. Soc. China* **2002**, *12*, 748–753.
27. Zhou, S.H.; Wang, Y.; Chen, L.Q.; Liu, Z.K.; Napolitano, R.E. Solution-based thermodynamic modeling of the Ni-Ta and Ni-Mo-Ta systems using first-principle calculations. *Calphad* **2009**, *33*, 631–641. [CrossRef]
28. Zhou, Y.; Wen, B.; Ma, Y.; Melnik, R.; Liu, X. First-principles studies of Ni-Ta intermetallic compounds. *J. Solid State Chem.* **2012**, *187*, 211–218. [CrossRef]
29. Kosorukova, T.; Firstov, G.; Noel, H.; Ivanchenko, V. Crystal structure changes in the Ni_3Ta intermetallic compound. *Chem. Met. Alloys* **2013**, *6*, 196–199.
30. Zhou, C.; Guo, C.; Li, C.; Du, Z. Thermodynamic optimization of the Ni-Ta system supported by the key experiments. *Thermochim. Acta* **2018**, *666*, 135–147. [CrossRef]
31. Pavlů, J.; Vřešťál, J.; Šob, M. Re-modeling of Laves phases in the Cr-Nb and Cr-Ta systems using first-principles results. *Calphad* **2009**, *33*, 179–186. [CrossRef]
32. Venkatraman, M.; Neumann, J.P. The Cr-Ta (chromium-tantalum) system. *J. Phase Equilib.* **1987**, *8*, 112–116. [CrossRef]
33. Okamoto, H. Cr-Ta (chromium-tantalum). *J. Phase Equilib.* **1996**, *17*, 457–457. [CrossRef]
34. Dupin, N.; Ansara, I. Thermodynamic assessment of the Cr-Ta system. *J. Phase Equilib.* **1993**, *14*, 451–456. [CrossRef]

35. Nash, P.; West, D.R.F. Nickel-rich region of Ni-Cr-Ta system at 1523 and 1273 K. *Met. Sci.* **1980**, *14*, 273–276. [CrossRef]
36. Schittny, S.U.; Lugscheider, E.; Knotek, O. Melting behaviour and phase equilibria in the system nickel-chromium-tantalum. *Thermochim. Acta* **1985**, *85*, 167–170. [CrossRef]
37. Nikolaev, S.V.; Balykova, Y.V.; Kerimov, E.Y.; Slyusarenko, E.M. Phase equilibria at 1375 K in three-component system of nickel-chromium-tantalum. *Moscow Univ. Chem. Bull.* **2013**, *68*, 23–28. [CrossRef]
38. Dupin, N.; Ansara, I. Theermodynamic assessment of the Cr–Ni–Ta system. *Z. Metallkd.* **1996**, *87*, 555–561.